Bulletin of the Seismological Society of America. Vol. 66, No. 5, pp. 1501–1523. October 1976

SCALING RELATIONS FOR EARTHQUAKE SOURCE PARAMETERS AND MAGNITUDES

BY ROBERT J. GELLER

ABSTRACT

A data set of 41 moderate and large earthquakes has been used to derive scaling rules for kinematic fault parameters. If effective stress and static stress drop are equal, then fault rise time, τ, and fault area, S, are related by $\tau = 16S^{1/2}/(7\pi^{3/2}\beta)$, where β is shear velocity. Fault length (parallel to strike) and width (parallel to dip) are empirically related by $L = 2W$. Scatter for both scaling rules is about a factor of two. These scaling laws combine to give width and rise time in terms of fault length. Length is then used as the sole free parameter in a Haskell type fault model to derive scaling laws relating seismic moment to M_S (20-sec surface-wave magnitude), M_S to S and m_b (1-sec body-wave magnitude) to M_S. Observed data agree well with the predicted scaling relation. The "source spectrum" depends on both azimuth and apparent velocity of the phase or mode, so there is a different "source spectrum" for each mode, rather than a single spectrum for all modes. Furthermore, fault width (i.e., the two dimensionality of faults) must not be neglected. Inclusion of width leads to different average source spectra for surface waves and body waves. These spectra in turn imply that m_b and M_S reach maximum values regardless of further increases in L and seismic moment. The m_b versus M_S relation from this study differs significantly from the Gutenberg-Richter (G-R) relation, because the G-R equation was derived for body waves with a predominant period of about 5 sec and thus does not apply to modern 1-sec m_b determinations. Previous investigators who assumed that the G-R relation was derived from 1-sec data were in error. Finally, averaging reported rupture velocities yields the relation $v_R = 0.72\beta$.

INTRODUCTION

The purpose of this paper is to examine empirical relations between gross fault parameters and the agreement of these relations with theoretical models of seismic sources. The gross parameters to be studied are fault length, width, and rise time, rupture velocity m_b and M_S, and seismic moment. Data from other investigators' studies of individual earthquakes are used to study scaling of source parameters in an approximate way. In general, the data are consistent with fault width scaling proportionately to fault length and rise time scaling proportionately to the square root of fault area. This scaling can then be used to find m_b-M_S, $\log M_o$-M_S and $\log S$-M_S relations. Some of those relations have been studied by Kanamori and Anderson (1975b), who provided a theoretical basis for many of the empirical relationships used in seismology.

Tsuboi (1956) was the first investigator to utilize similarity, the concept of relating earthquakes of different sizes by a one-parameter model. By assuming that the horizontal dimensions of the earthquake source volume were three times larger than the vertical dimension, Tsuboi derived from the relation $E = \mu\varepsilon^2 A^{1.5}/6$, where E is released energy, μ is average rigidity, ε is average strain drop and A is aftershock area. Such approximate scaling relations, as first pointed out by Tsuboi, require that the physics of material failure be identical for large and small earthquakes. If that assumption is generally true and if earthquakes tend to be geometrically similar, then it follows that fault length and width,

TABLE 1

EARTHQUAKE SOURCE PARAMETERS

Event	Date	M_S	m_b	M_o $\times 10^{27}$ dyne-cm	L (km)	W (km)	$\bar{D}$ (m)	τ (sec)	τ^* (sec)	V_R (km/sec)	$\Delta\sigma$ (bars)
1. Kanto	1 Sep. 1923	8.2	—	7.6	130	70	2.1	7	10	—	21
2. Tango	27 Mar. 1927	7.75	—	0.46	35	13	3	6	2.5	2.3	115
3. North Izu	25 Nov. 1930	7.1	—	0.2	20	11	3	—	1.7	—	150
4. Saitama	21 Sep. 1933	6.75	—	0.068	20	10	1	2	1.6	2.3	59
5. Sanriku	2 Mar. 1933	8.3	—	43	185	100	3.3	7	12	3.2	42
6. Long Beach	11 Mar. 1933	6.25	—	0.028	30	15	0.2	2	2.5	2.3	7
7. Imperial Valley	19 May 1940	7.1	—	0.48	70	11	2	—	3.2	—	55
8. Tottori	10 Sep. 1943	7.4	—	0.36	33	13	2.5	3	4.0	2.3	99
9. Tonankai	7 Dec. 1944	8.2	—	15	120	80	3.1	—	9.2	—	39
10. Mikawa	12 Jan. 1945	7.1	—	0.087	12	11	2.2	—	1.3	—	140
11. Nankaido	20 Dec. 1946	8.2	—	15	120	80	3.1	—	9.2	—	39
12. Fukui	28 Jun. 1948	7.3	—	0.33	30	13	2	2	1.9	2.3	100
13. Tokachi-Oki	4 Mar. 1952	8.3	—	17	180	100	1.9	—	14	—	17
14. Kern County	21 Jul. 1952	7.7	—	2	60	18	4.6	1	3.6	—	140
15. Fairview	16 Dec. 1954	7.1	—	0.13	36	6	2	—	1.7	—	100
16. Chile	22 May 1960	8.3	—	2400	800	200	21	—	36	3.5	91
17. Kitamino	19 Aug. 1961	7.0	—	0.09	12	10	2.5	2	1.3	3.0	170
18. Wasaka Bay	27 Mar. 1963	6.9	—	0.033	20	8	0.6	2	1.5	2.3	40

19.	North Atlantic I	3 Aug. 1963	6.7	6.1	0.12	32	11	1	—	2.2	—	44
20.	Kurile Islands	13 Oct. 1963	8.2	5.7	75	250	140	3	—	17	3.5	28
21.	North Atlantic II	17 Nov. 1963	6.5	5.9	0.038	27	9	0.48	—	1.8	—	24
22.	Spain	15 Mar. 1964	7.1	6.2	0.13	95	10	0.42	—	3.6	1.4	11
23.	Alaska	28 Mar. 1964	8.5	6.2	520	500	300	7	—	35	3.5	22
24.	Niigata	16 Jun. 1964	7.4	6.1	3.2	80	30	3.3	—	5.3	—	66
25.	Rat Island I	4 Feb. 1965	7.9	6.0	140	500	150	2.5	—	25	4.0	17
26.	Rat Island II	30 Mar. 1965	7.5	5.7	3.4	50	80	1.2	—	5.8	—	33
27.	Parkfield	28 Jun. 1966	6.4	5.3	0.032	26	7	0.6	0.7	1.6	2.7	32
28.	Aleutian	4 Jul. 1966	7.2	6.2	0.226	35	12	1.6	—	2.4	—	64
29.	Truckee	12 Sep. 1966	5.9	5.4	0.0083	10	10	0.3	—	1.2	—	20
30.	Peru	17 Oct. 1966	7.5	6.3	20	80	140	2.6	—	9.6	—	41
31.	Borrego	9 Apr. 1968	6.7	6.1	0.063	33	11	0.58	—	2.2	—	22
32.	Tokachi-Oki	16 May 1968	8.0	5.9	28	150	100	4.1	—	12	3.5	37
33.	Saitama	1 Jul. 1968	5.8	5.9	0.019	10	6	0.92	1	0.9	3.4	100
34.	Portuguese	28 Feb. 1969	8.0	7.3	5.5	80	50	2.5	—	6.1	—	53
35.	Kurile Islands	11 Aug. 1969	7.8	7.1	22	180	85	2.9	—	12	3.5	28
36.	Gifu	9 Sep. 1969	6.6	5.5	0.035	18	10	0.6	1	1.7	2.5	35
37.	Peru	31 May 1970	7.8	6.6	10	130	70	1.6	—	8.7	2.5	28
38.	San Fernando	9 Feb. 1971	6.6	6.2	0.12	20	14	1.4	1	2.0	2.4	62
39.	Nemuro-Oki	17 Jun. 1973	7.7	6.5	6.7	60	100	1.6	—	7.5	—	35
40.	Turkey	22 Jul. 1967	7.1	6.0	0.83	80	20	1.7	—	4.7	—	32
41.	Iran	31 Aug. 1968	7.3	5.9	1	80	20	2.1		4.7	—	38

REFERENCES TO TABLE 1

(1) Kanamori (1971a). Rise time from Kanamori (1974).
(2) Kanamori (1973).
(3) Average of Chinnery (1964), Kasahara (1957) and Kanamori (unpublished data).
(4) Abe (1974b).
(5) Average of Kanamori (1971b) and Kawasaki and Suzuki (1974).
(6) Kanamori (unpublished data) and aftershock zone.
(7) Average of Brune and Allen (1967) and Byerly and DeNoyer (1958).
(8) Kanamori (1972b).
(9) Kanamori (1972a).
(10) Ando (1974).
(11) Kanamori (1972a).
(12) Kanamori (1973).
(13) Area from average of Kanamori (unpublished data) and Utsu and Seki (1954). Moment from Kanamori (unpublished data).
(14) Kanamori (unpublished data).
(15) Savage and Hastie (1966).
(16) Average (for main shock only—precursor not included) of Kanamori and Cipar (1974) and Kanamori and Anderson (1975a).
(17) Kawasaki (1975).
(18) Abe (1974a).
(19) Udias (1971).
(20) Kanamori (1970a).
(21) Udias (1971).
(22) Udias and Arroyo (1970).
(23) Kanamori (1970b).
(24) Abe (1975a).
(25) Wu and Kanamori (1973).
(26) Abe (1972a).
(27) Average of Anderson (1974) and Trifunac and Udwadia (1974).
(28) Udias (1971).
(29) Tsai and Aki (1970).
(30) Abe (1972b).
(31) Hanks and Wyss (1972).
(32) Kanamori (1971c).
(33) Abe (1975b).
(34) Fukao (1973).
(35) Abe (1973).
(36) Mikumo (1973a).
(37) Abe (1972b). Average of parameters for each of the two possible fault planes.
(38) Moment and static fault parameters from Kanamori and Anderson (1975b). Rupture velocity and rise time averaged from Boore and Zoback (1974), Mikumo (1973b) and Trifunac (1974).
(39) Shimazaki (1975).
(40) Hanks and Wyss (1972).
(41) Hanks and Wyss (1972).

and final dislocation all will scale together. Differences in material properties will weaken the exactness of the similarity when earthquakes from two different regions are compared, but, in an approximate sense, similarity, as is shown by the data presented below, is a valid concept.

The first paper to systematically relate observed gross seismic source parameters to the source spectrum was the now classic work of Aki (1967). Although the results presented in this paper modify his results, the methodology and basic outlook are similar to Aki's. Later Brune (1970, 1971) contributed to the understanding of seismic source spectra.

Similarity between earthquakes is a dynamic as well as a static concept. Not only the final static parameters, but also the spectral shape of the equivalent source-time function, scale with fault length. Spectral similarity can best be demonstrated by comparing two earthquakes with identical location and focal mechanism, but different magnitude. Such a comparison ensures that seismograms from both events will be affected equally by the medium response, so that all differences between the records will be from the source effects.

Observational studies of similar pairs of earthquakes have been made by Berckhemer (1962) whose results were interpreted by Aki (1967) to support Aki's ω^{-2} model. Tsujiura (1973) studied groups of events from various regions, concluding that most data were in accord with Aki's ω^{-2} model, but that some were better fit by an ω^{-1} or ω^{0} model.

One cannot directly compare spectral characteristics of source mechanisms from different regions without first correcting the seismograms for transmission effects. Removing the effects of medium response will usually require use of synthetic seismogram methods. We assume however that one can compare logarithmic fault parameters, such as m_b, M_S or $\log L$, for events in different regions. These comparisons are made with the intention of looking at order of magnitude relationships rather than details.

In this paper, we will look at scaling relations between five sets of such logarithmic parameters: $\log L$ versus $\log W$ (fault length versus width), $\log \tau$ versus $\log S$ (fault rise time versus area), M_S versus $\log M_o$ (surface-wave magnitude versus seismic moment), m_b versus M_S and $\log S$ versus M_S. What will be shown are not exact correlations, but rather trends which appear to be applicable to most earthquakes. Agreement between the simple model used in this paper and the data are quite good. (Long narrow transform faults, such as the San Andreas, are a separate class of faults which are not considered in this paper.)

Observational Data Set

The earthquake data shown in Table 1 are from the same 41 shallow events used by Kanamori and Anderson (1975b). All values for M_S are from their paper; the sources for all other observational parameters are given in the table of references. Except for minor differences which are primarily due to the use of slightly different references, data for M_o and S are equivalent to that of Kanamori and Anderson (1975b). Each numbered entry in the table of references corresponds to the earthquake with the same number in Table 1. All but two of the columns are observational data; τ^*, predicted rise time, and $\Delta\sigma$, calculated stress drop, will be discussed below. Length and width have been taken from the references, or in some cases estimated. Length always refers to length along the strike, regardless of focal mechanism; width refers to width along the dip. Average dislocation comes either from field measurements or from dividing the moment (determined from seismograms) by the area and an assumed value of the shear modulus.

For all events since August 1963 the m_b value is either taken directly from the *PDE Monthly Summary*, or calculated from the data in *Earthquake Data Reports*. As reported by L. M. Murphy in Båth (1969), USCGS (later NOAA and now USGS) asks for the amplitude of the largest pulse (with period less than 3 sec) in the first five cycles of the teleseismic P or P_n arrival. The values of A and T are then used in the Gutenberg-Richter formula

$$m_b = \log_{10}(A/T) + Q, \tag{1}$$

to derive m_b for each station. Values more than 0.7 magnitude units from the mean are deleted and the final average is then taken.

Estimates of rise times typically were made by fitting the first upswing on long-period local records to synthetic seismograms calculated using the Haskell (1969) whole-space model at one or two stations. Clearly it would be desirable to use synthetics made for more realistic models of earth structure, but they have not yet been calculated for these events. Uncertainties due to the tradeoff between rise time and rupture velocity and due to the model may combine to cause errors which cannot be estimated. In some cases, such as the Tottori earthquake (Kanamori, 1972b), rupture velocity and rise time are independently constrained.

Length versus Width

Fault length is plotted against fault width in Figure 1. It can be seen that (with considerable scatter) observational data demonstrate that $L = 2W$. In Figure 1, the

numbers refer to earthquakes in Table 1. Intraplate events are plotted as open circles and interplate events as solid circles. (This convention is also used in all later figures.) There is not any clear difference between the interplate and intraplate groups. Abe (1975c) has independently found $L=2W$ for a data set of mainly Pacific earthquakes.

The Haskell model uses L as the direction in which rupture propagates, while L was measured along the direction of the strike for Figure 1. It is implicitly assumed, then, that for these 41 events, rupture propagated parallel to the strike. This almost certainly is false for some thrust events such as San Fernando (Boore and Zoback, 1974; Trifunac, 1974; Mikumo, 1973b), and may well be false for events like Nemuro-Oki with $L<W$. In spite of these exceptions it seems that rupture usually propagates parallel to the strike, especially for strike-slip faults.

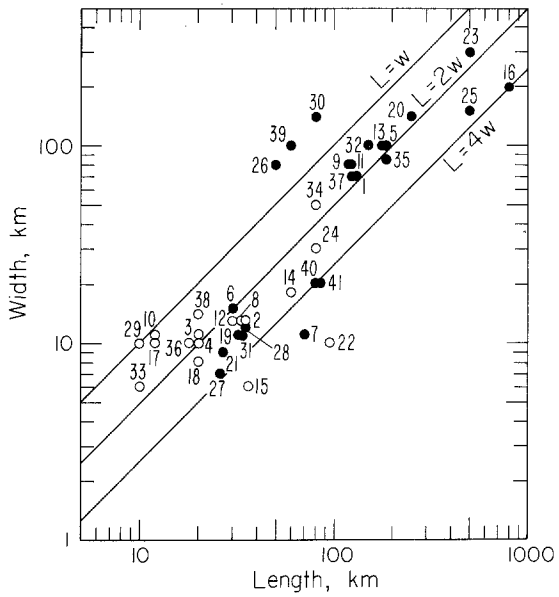

FIG. 1. Plot of fault length (along strike) versus fault width (along dip) for earthquakes in Table 1. Open circles are intraplate events; closed circles are interplate events. Numbers refer to Table 1. These conventions are used for all plots of earthquake data.

RISE TIME VERSUS THEORETICAL PREDICTIONS

Kanamori (1972b) showed that

$$\dot{D}=\frac{\bar{D}}{\tau}\cong\sigma_{e,o}\frac{\beta}{\mu} \tag{2}$$

where $\dot{D}$ is dislocation velocity, $\bar{D}$ is average dislocation, τ is rise time, and $\sigma_{e,o}$ is effective stress. If one assumes that effective dynamic stress is equal to static stress drop, $\Delta\sigma$, this assumption can be tested by comparing observed rise times to the theoretically predicted rise time

$$\tau^*=\frac{\mu\bar{D}}{\beta\Delta\sigma}. \tag{3}$$

One can obtain stress drop in closed form for only a few simple models. The most straightforward of these is the circular crack with constant stress drop discussed by Keiles-Borok (1959). For that model stress drop is given by

$$\Delta\sigma=7\pi^{3/2}\mu\bar{D}/(16\sqrt{S})=7M_o/(16(LW/\pi)^{3/2}). \tag{4}$$

Although this formula does not give the exact stress drop for the rectangular fault model, it follows from the work of Sato (1972) that this is a good approximation. If we substitute (4) in (3), where S is the area of the rectangular fault and $\bar{D}$ is average dislocation, we obtain

$$\tau^* = 16S^{1/2}/(7\pi^{3/2}\beta). \tag{5}$$

The values of $\Delta\sigma$ and τ^* in Table 1 were calculated using (4) and (5), respectively.

Figure 2 is a plot of observed versus predicted [from (5)] rise times for a number of earthquakes. It can be seen that, again with considerable scatter, observational and theoretical rise times are in agreement. Abe (1975b) reached a similar conclusion from a data set of five Japanese earthquakes.

The agreement between theoretical and observed rise times has important implications for engineering seismology. The only observational parameter required in (5) is fault area, which frequently can be estimated from geological data. If total dislocation can also be

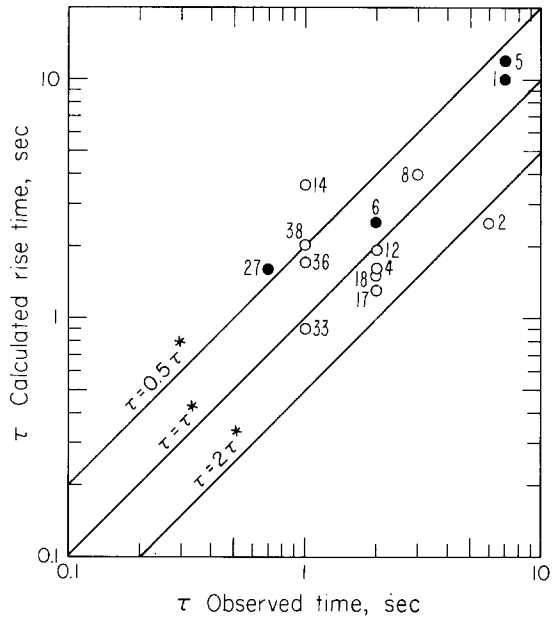

FIG. 2. Plot of observed rise time versus theoretical rise times from (5).

determined from geological field work, then particle velocity near the fault, an important parameter in engineering seismology, can be reliably estimated. This is potentially of great value in areas lacking in historical seismicity or good instrumental data.

RUPTURE VELOCITY

Table 1 lists rupture velocities reported by various investigators. These values were determined from matching synthetic seismograms to local records or from surface-wave analysis. To a certain extent then, these values are model-dependent. Some also may be affected by the difficulty in resolution between rise time and rupture velocity. Nevertheless, these measurements probably represent a good average sample of rupture velocity measurements. If one picks values of β ranging from 3.5 km/sec for shallow crustal events to 4.5 km/sec for events breaking the entire lithosphere, one then can calculate that the average value of (v_R/β) is 0.72.

Archuleta and Brune (1975) found $v_R/\beta = 0.7$ in experiments on fracture of prestressed foam rubber. Their measured value was for the surface of the foam rubber, but if one assumes infinite rupture velocity along the dip, their result agrees very well with the result $v_R/\beta = 0.72$ observed for earthquakes. (Their minimum possible value for v_R/β at depth is 0.63β.) Agreement between the earthquake and foam rubber rupture velocities may be fortuitous or may be caused by a common physical friction mechanism.

Choice of Fault Models

All "deterministic" source models specify some (nearly always kinematic) conditions at the source, which then fix via the representation theorem of de Hoop (1958) and Burridge and Knopoff (1964), the complete time history at every point in the medium. [Aki (1967, 1972) and Haskell (1966) proposed "statistical" models in which only the amplitude spectrum at the source function is specified. Since we will be looking at dislocation rise times, these statistical models are not appropriate choices.] Typically the source theory papers calculate seismograms for an isotropic homogeneous whole space. Since our interest is in logarithmic source parameters, we will assume the whole-space models are adequate.

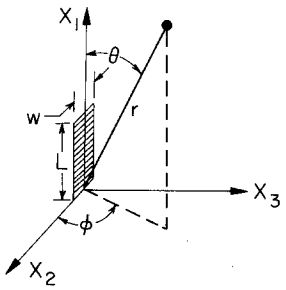

FIG. 3. The Haskell (whole space) fault model.

In most deterministic source models, either fault dislocation (e.g., Haskell, 1969, and Mikumo, 1973b) or stress drop [and therefore fault dislocation, e.g., Burridge and Willis (1969), Richards (1973), Sato and Hirasawa (1973)], is specified, which in turn gives displacement at other points in the medium. Other authors, e.g., Hanson *et al.* (1974) and Andrews (1975), have studied numerical models with friction between the fault surfaces.

All of these models predict far-field pulses which scale linearly with fault dimensions. Also they all yield flat spectra at low frequencies and ω^{-n} high-frequency asymptotes ($n \geqq 2$). Thus all of the models have at least one "corner frequency" (and some have several). For these models the static or low-frequency level, which is proportional to seismic moment, grows as L^3.

We will continue to use the Haskell (1964, 1969) model of a rectangular fault (shown in Figure 3) in this paper. Most studies have used this model in the determination of rise times from local seismograms. The basic Haskell model is a fault with length L, width W, rise time τ (linear ramp time function), final dislocation $\bar{D}$ and rupture velocity V_R. Rupture is instantaneous in the width direction and propagates (starting at one end) along the length with velocity v_R. Some investigators have made the natural extension to bilateral rupture propagation.

Haskell's (1964) expressions are for a "one-dimensional" model in which width is included only as a weighting factor in the moment. Hirasawa and Stauder (1965) and

Mikumo (1969) included the complete effect of the width to obtain an expression for spectral source amplitude.

$$|u_c(\omega)| = \frac{M_o R^c_{\theta\phi}}{4\pi\rho r c^3} \left| \frac{\sin(\omega\chi_\tau)}{\omega\chi_\tau} \right| \left| \frac{\sin(\omega\chi_L)}{\omega\chi_L} \right| \left| \frac{\sin(\omega\chi_W)}{\omega\chi_W} \right|. \tag{6}$$

In (6) M_o is moment, ρ is density, r is distance, c is either P or S velocity and $R^c_{\theta\phi}$ is the radiation pattern (given by Haskell, 1964). χ_L and χ_W are duration times associated with length and width, respectively, and determined by fault geometry and position of the observer.

$$\chi_L = |L(1/v_R - \cos\theta/c)/2| \tag{7}$$

$$\chi_W = |W(\cos\phi \sin\theta)/(2c)| \tag{8}$$

$$\chi_\tau = \tau/2. \tag{9}$$

Spectral Characteristics

For the present, let us adopt (in slightly modified form) the similarity relations given by Kanamori and Anderson (1975b).

$$\frac{W}{L} = C_1 = \text{const} \tag{10}$$

$$\frac{\bar{D}}{L} = C_2 = \text{const} \tag{11}$$

$$\frac{\beta\tau}{L} = C_3 = \text{const} \tag{12}$$

(10) is the condition of geometrical similarity; (11) and (12) imply constant stress drop and constant effective stress.

We will select values of the constants which seem to be good averages of observational data. We found that

$$L = 2W \tag{13}$$

seemed to be the approximate average of the empirical data. When we substitute $L = 2W$ into (5) and set $\beta = 4.0$ km/sec we get

$$\tau = [16\sqrt{L^2/2}/(7\pi^{3/2} \cdot 4)] = 0.0726L \tag{14}$$

where τ is in seconds and L is in kilometers.

We could use (11) directly to get a scaling relation between fault displacement and length. In practice though, most estimates of $\bar{D}$ in Table 1 come from dividing M_o by μS, so it seems better to relate moment directly to length. Setting $L = 2W$ in (4) gives moment in terms of fault length and stress drop.

$$M_o = L^3 \Delta\sigma \cdot 16/(7(2\pi)^{3/2}) = (1.45 \times 10^{20}) L^3 \Delta\sigma \tag{15}$$

where M_o is in dyne centimeters, L is in kilometers and $\Delta\sigma$, in bars.

From (6) we can isolate a spectral factor, dependent only on fault parameters and frequency.

$$A(\omega) = L^3 \left| \frac{\sin(\omega\chi_\tau)}{\omega\chi_\tau} \right| \left| \frac{\sin(\omega\chi_L)}{\omega\chi_L} \right| \left| \frac{\sin(\omega\chi_W)}{\omega\chi_W} \right| \tag{16}$$

The L^3 term follows from the similarity relation $M_o \sim L^3$. When $A(\omega)$ is multiplied by stress drop and the constant in similarity equation (15) we get the source moment rate spectrum.

Equation (16) and the factors (7) to (9) are well-known results for the case of a rectangular fault in a whole space. These expressions can also be applied directly to the case of a rectangular fault with horizontal rupture propagation in the Earth. The form of the expressions remains identical, but c now should be interpreted as the apparent velocity along the Earth's surface.

For body waves $c = v_c/\sin i$, where v_c is the near-field P or S velocity and i is the takeoff angle of the teleseismic ray from the focal sphere. This can be understood physically by invoking reciprocity. Signals from a source at the position of the teleseismic receiver would be picked up $(L \cos\theta)/(2c)$ sooner at the end of the fault than at the center. Thus for the case of infinite rupture velocity, this is the difference between arrivals at the receiver from the end and center of the fault. This type of geometrical interpretation can be applied to both (7) and (8), so that these factors are seen to be the difference in arrival times obtained from geometrical optics. Ben-Menahem (1962) gives a more rigorous derivation of this result.

For surface waves (7) is the well-known directivity factor first given by Ben-Menahem (1961). If we neglect the variation of the excitation function with depth, (8) is the factor for the effect of fault width on the surface-wave spectrum. In both (7) and (8), c is the (frequency-dependent) surface-wave phase velocity. The geometrical interpretation of (7) and (8) as phase delay between "arrivals" from the center of the fault and the ends is the same as for body waves.

Typical values of c for teleseismic P waves might be 14 km/sec, while for surface waves 4 km/sec is appropriate. If rupture velocity, $v_R = 2.5$ km/sec, then for surface waves $1/c$ will be of the same order of magnitude as $1/v_R$. As θ varies from 0 to 2π, χ_L will range from $0.15\,L$ to $0.65\,L$. Thus a horizontally propagating rupture will cause a large directivity effect. On the other hand, for body waves from the same source, $\cos\theta = \sin i$, so because of the relatively steep takeoff angles of teleseismic rays, it is reasonable to assume $|\cos\theta| < 0.5$.

This assumption leads to the conclusion that χ_L will vary only from $0.36\,L$ to $0.44\,L$. There will be only a small azimuthal dependence (i.e., directivity effect) of the teleseismic body-wave pulse. This implies that one can infer the nature of a horizontal rupture propagation much more easily from surface waves than teleseismic body waves.

Because c is the apparent velocity, rather than the near-field P or S velocity, it is inadequate to present only a single spectrum representing the effect of the seismic source, as was done, for example, by Aki (1967, 1972). There is a separate "source spectrum," $A(\omega)$, for each body-wave phase or surface-wave mode, because of the different values of c. The source spectrum depends on azimuth, source dimensions, and the phase velocity, c. Both the length factor, (7), and the width factor, (8), are different for each mode. In the next section we will average χ_L and χ_W over all azimuths. In these averages, the value of c will affect only χ_W, even though both factors are affected at nearly every particular azimuth.

Both (6) and (16) completely neglect the effect of the Earth's transfer function on observed seismic waves. If one were to calculate synthetic seismograms for an individual earthquake, it would be necessary to consider the Earth's response and the earthquake source parameters, e.g., Langston and Helmberger (1975) for body waves or Harkrider (1964, 1970) for surface waves. Langston and Helmberger (1975) have demonstrated that sP and pP phases play a crucial role in the "P wave" from shallow earthquakes. Similarly, one must consider the surface-wave excitation functions and the source mechanism to calculate accurate Rayleigh and Love amplitudes.

In this paper we consider trends among events, rather than accurate determination of parameters of particular events. Therefore, we assume that the effect of the earth structure

averages out when we construct scaling relations. Thus we will use (16) to get relations between m_b and M_S, $\log L$ and M_S, $\log M_o$ and M_S.

Average Spectra

We now want to find average asymptotic forms for $\log A(\omega)$ from (16). In particular we require expressions for teleseismic P phases (from which m_b will be determined) and for 20-sec Rayleigh waves (from which we find M_S). For both cases we will find average values of χ_L and χ_W which take the direction of radiation into account. In making our approximation, we will replace $|(\sin X)/X|$ by one for $X<1$ and by X^{-1} for $X \geqq 1$.

Takeoff angles of teleseismic body waves are nearly vertical. We will adopt the approximation that the rays take off straight down. Thus, for body waves, we set $\theta = \pi/2$ in (7) and (8). Also, in that case, $|\cos\phi| = \sin\delta$, where δ is dip angle of the fault plane. Using these values, average spectral factors for body waves are

$$\langle \chi_L \rangle_{\text{body}} = L/(2v_R) \tag{17}$$

and

$$\langle \chi_W \rangle_{\text{body}} = W \sin\delta/(2c). \tag{18}$$

For surface waves we will average χ_L and χ_W for $\theta = 0$ to $\theta = 2\pi$. On the Earth's surface we get $|\cos\phi| = \cos\delta$. Thus we get

$$\langle \chi_L \rangle_{\text{surf}} = L/(2V_R) \tag{19}$$

and

$$\langle \chi_W \rangle_{\text{surf}} = W \cos\delta/(\pi c). \tag{20}$$

Comparison of (17) and (18) with (19) and (20) shows that the average corner frequency due to fault length will be the same for body waves and surface waves, but that the corner frequencies due to width will be different. This difference affects the high-frequency spectrum only since the average corner frequency for width is higher than that for rise time or length. Note that we have assumed that rupture propagates parallel to the Earth's surface to obtain (17) to (20).

Before calculating numerical values for (17) to (20) we must fix v_R, δ and c. Also we will use (13) to relate L to W. We will set $v_R = 2.88$ km/sec, $\delta = 45°$, $c = 14$ km/sec for body waves and $c = 3.9$ km/sec for surface waves. (For the Earth, c must be the appropriate phase velocity, not the S-wave velocity. Neglecting the frequency dependence of surface-wave phase velocity is a reasonable approximation.)

From (9) and (14)

$$\chi_\tau = 0.0363\, L = C_\tau L \tag{21}$$

(17) and (19) both give

$$\langle \chi_L \rangle = 0.174\, L = C_L L. \tag{22}$$

The width factor for body waves is

$$\langle \chi_W \rangle_{\text{body}} = 0.0126\, L = C_{Wb} L. \tag{23}$$

For surface waves we get

$$\langle \chi_W \rangle_{\text{surf}} = 0.0289 L = C_{Ws} L. \tag{24}$$

We now can approximate the logarithm of $A(\omega)$ from (16).

$$\begin{aligned}
&\log A(\omega) = 3 \log L && \text{for} \quad \omega < (C_L L)^{-1} \\
&\log A(\omega) = 2 \log L - \log \omega - \log C_L && \text{for} \quad (C_L L)^{-1} < \omega < (C_\tau L)^{-1} \\
&\log A(\omega) = \log L - 2 \log \omega - \log (C_L C_\tau) && \text{for} \quad (C_\tau L)^{-1} < \omega < (C_W L)^{-1} \\
&\log A(\omega) = -3 \log \omega - \log (C_L C_\tau C_W) && \text{for} \quad (C_W L)^{-1} < \omega.
\end{aligned} \tag{25}$$

The spectra from these relations are plotted in Figure 4. Note that the body-wave spectra have a much longer interval of ω^{-2} decay then the surface-wave spectra. Calibration of these curves with M_S and M_o is discussed below. Also, note that ω is in radians in (25), but in hertz in Figure 4.

The asymptotic spectral amplitudes given by (25) are very similar to the results obtained by Kanamori and Anderson (1975b). They used the same asymptotic approximation for

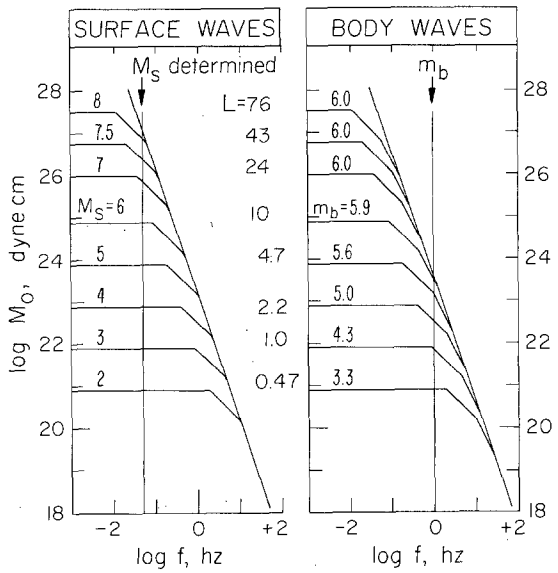

FIG. 4. Source spectra of surface waves (on left) and body waves. Both are identical at frequencies below the ω^{-2} corner frequency. The body waves have a higher width corner frequency than surface waves, which follows from (18), (20), (23) and (24). This difference occurs because teleseismic P waves, which take off essentially straight down, have a much higher apparent velocity (phase velocity) than surface waves. Therefore the separation between rise time and width corner frequencies (the ω^{-2} part of the spectrum) is much greater for body waves than for surface waves.

$\sin X/X$ in conjunction with Haskell's (1964) spectral expression. Since Haskell's expression ignores the effect of width on the spectrum, the results of this paper differ from those of Kanamori and Anderson (1975b) only at frequencies above the corner frequency for width. For example, the model in this paper predicts constant 20-sec spectral amplitude for faults longer than 110 km while that of Kanamori and Anderson (1975b) predicts amplitudes which increase linearly with L. As a result, their model predicts $M_S \sim \log L$ for large events, while this paper predicts $M_S = \text{const}$.

Even though both spectra in Figure 4 have an eventual ω^{-3} asymptote, they are quite different than Aki's (1967) ω-cube model. Aki's models, as a result of his assumption that $vk_L = k_T$, had only a single corner frequency. His ω-cube model makes a fairly abrupt transition from ω^0 to ω^{-3} behavior. The spectra presented here, particularly the body-wave spectrum, show a gradual transition from ω^0 to ω^{-3} asymptotes.

m_b-M_S relation. Changes in the definition of the body-wave magnitude scale have resulted in a large amount of confusion today. Gutenberg and Richter (1942) extended the body-wave magnitude scale from local events to fairly distant events which were recorded on Wood-Anderson and strong-motion torsion instruments.

Gutenberg (1945) introduced a scheme for m_b differing only in minor details from the summary in Richter (1958). He determined m_b from the instruments available in 1945, which were mostly broad-band mechanical types. Gutenberg (1945) stated that "the average period of P waves in teleseisms is about 4 to 6 sec." In general, Gutenberg did not publish the period of the P waves he used in determining m_b, but from a preliminary examination of his unpublished data it seems that many of his amplitudes were obtained at periods of 4 to 10 sec.

Gutenberg and Richter (1956) published their final version of the relation between m_b and M_S

$$m_b = 0.63\, M_S + 2.50 \tag{26a}$$

$$M_S = 1.59\, m_b - 3.97. \tag{26b}$$

Their primary reason for deriving this relation was to facilitate the construction of a "unified magnitude scale." Investigators at that time apparently viewed the discrepancy between the two magnitude scales as an experimental error, rather than a fundamental effect of the seismic source spectrum. This view was not unreasonable at the time because m_b was measured at periods differing only by a factor of 2 to 5 from M_S and modern source theories had not yet been developed. In any case, Gutenberg and Richter found the (body wave) magnitude m_S, corresponding to a given M_S, by using (26a). They then took a weighted average of m_b, the actual body-wave magnitude, and m_s to obtain m, the unified magnitude. Later Richter (1958) published values of unified (surface wave) magnitude, M, which he obtained by converting m to M using (26b). In retrospect, unified magnitude was inappropriate, since it now is clear that for all seismic source theories m_b and M_S represent different parts of the spectrum which are not related by a factor independent of fault length.

m_b determinations by the USCGS (later NOAA and now the USGS) differ markedly from those used by Gutenberg and Richter. USCGS values for m_b use (1), but A and T are measured on the WWSSN short-period instrument, which is sharply peaked at 0.5 sec. T nearly always is about 1 sec in WWSSN magnitude determinations. Thus WWSSN magnitudes are based roughly on 1-sec spectral amplitude. On the other hand, Gutenberg and Richter determined m_b for many events at about 5 sec, with even larger T for the largest events. Therefore, it is wrong to take the Gutenberg-Richter m_b as being related to spectral amplitude at any one particular period.

Modeling m_b-M_S. Aki (1967) proposed two statistical models of seismic sources, an "ω-square" model (which decayed as ω^{-2} at high frequencies) and an "ω-cube" model, after Haskell (1966) (which decayed as ω^{-3}). Aki compared these two models by calculating spectral ratios for similar events and by calculating the relation of m_b to M_S predicted by each model.

Aki calculated M_S by adding a constant to the logarithm of spectral amplitudes at 20 sec. The constant was chosen to give the best agreement between theoretical and observational spectral ratios of pairs of similar earthquakes studied by Berckhemer (1962). After fixing the additive constant for M_S, Aki then defined a similar relation for m_b. He set $m_b = \text{const} + (0.71 \sim 0.83) \log A\,(1\text{ sec})$ and found the constant which would make $m_b = M_S$ when $M_S = 6.75$. The coefficient of $\log A$ (1 sec) comes from a correction for duration.

Aki (1967) calibrated his curves for the ω-square and ω-cube models in this way. He

then compared the m_b-M_S curves predicted by the models to the Gutenberg-Richter m_b-M_S relation (26). He suggested that the excellent agreement of the ω-square model with (26) strongly supported it, over the ω-cube model. Unfortunately, his theoretical m_b-M_S curve was based on 1-sec spectral amplitudes, while (26) was derived from mostly 4- to 10-sec data. Actually it seems that Aki's support for the ω-square model was incorrect. The WWSSN m_b-M_S data (based on 1-sec m_b), discussed below, disagree with the ω-square model.

The approach in this paper is to match m_b-M_S, log S-M_S, log M_o-M_S and spectral ratio data simultaneously, adjusting the two free parameters to get good overall agreement with the data. A least-squares solution is not particularly appropriate because of the large number of parameters and the lack of similarity (e.g., different stress drops) found when earthquakes are examined in detail.

m_b is approximated by a constant plus log A (1 sec) and M_S by another constant plus log A(20 sec). $A(\omega)$ was found using (25) with the constants in (21) to (24). After several

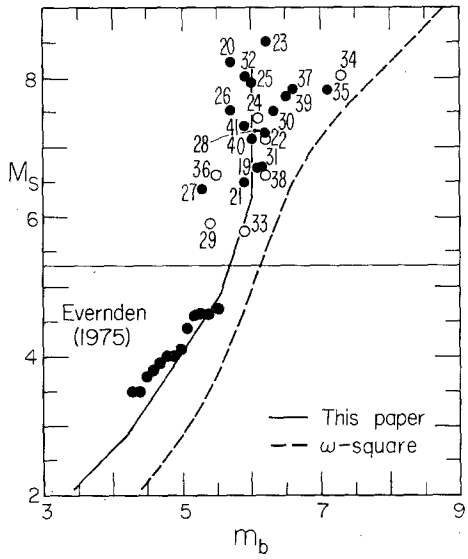

FIG. 5. USCGS m_b versus M_S. Lower data points are averages from Evernden (1975), corrected by adding 0.3 to m_b. Upper points (above horizontal line) are individual earthquakes from Table 1. Dashed curve is m_b-M_S relation from ω-square model. Solid curve is from (21) to (25) as described in the text.

trials the additive constants for m_b and M_S were determined to be $C_{m_b} = 4.30$ and $C_{M_S} = 2.97$. To obtain seismic moment as a function of L, it was necessary to assign $\Delta\sigma$ for use in (15). Kanamori and Anderson (1975b) found that stress drops are 10 to 30 bars for most interplate earthquakes and 30 to 100 bars for most intraplate earthquakes, so $\Delta\sigma = 50$ bars was used.

Clearly it is not exactly correct to get m_b and M_S directly from spectral amplitudes. A more accurate approach would be computing synthetic seismograms and then measuring m_b and M_S as it is done for data. For this study, using spectral amplitudes seems to be an acceptable approximation.

Archambeau (1975) thoroughly discussed the differences between time-domain and frequency-domain estimates of m_b and M_S. His study stressed the very small differences which are crucial in the context of seismic discrimination. In general though, his study supports the applicability of using spectral amplitudes to estimate m_b of small and

moderate events. Probably any discrepancy between spectral amplitudes and time-domain amplitudes is most severe for larger events.

m_b-M_S data. Two kinds of m_b-M_S data are plotted in Figure 5. Points below the solid line midway up the figure are from a study of almost one thousand events by Evernden (1975). Each point is the average value of M_S for all earthquakes with that m_b value. Because Evernden's m_b values are an average of 0.3 lower than the USGS values, 0.3 is added to the m_b values before plotting them. Points above the line are values for individual events since mid-1963 as listed in Table 1.

Data shown in Figure 5 are in general agreement with a study of the m_b-M_S relation by Nagamune (1972). Nagamune fitted two straight lines to 2 years of WWSSN m_b-M_S data. He found

$$M_S = 1.89\, m_b - 4.62 \qquad M_S > 5.73$$

and

$$M = 1.05\, m - 0.02 \qquad M < 5.73.$$

The latter equation comes from a study of small events mostly in Hokkaido. Magnitudes in the latter equation are very similar to m_b and M_S.

m_b-M_S curves from two models are plotted in Figure 5. The curve on the right is the m_b-M_S relation predicted by Aki (1972), which is based just on $\log A(1)$, without any correction for duration. It can be seen that all of the data lie substantially to the left (smaller m_b) of the ω-square curve. Inclusion of a duration correction for large events would not affect the basic conclusion that the ω-square model does not agree at all with the data.

The left-hand curve is derived from the Haskell model presented in this paper. It can be seen that the predicted m_b-M_S curve is generally in good agreement with the data. It would have been better to have averaged the value of m_b for all earthquakes with a particular M_S for all WWSSN events for several years, rather than present just a few data points.

The Evernden (1975) data have a slope of one for events with m_b smaller than $5\frac{1}{4}$ while the predicted m_b-M_S curve has a slope of $\frac{3}{2}$ for $m_b > 4.2$, which clearly disagrees with the data. The large events are too scattered to warrant a definite conclusion, but the predicted maximum m_b of 6.0 is probably 0.3 or 0.4 too small. This discrepancy may be due to use of spectral amplitudes instead of time-domain amplitudes. Also, it was assumed above that m_b was always based on 1-sec observations, but this is not strictly true. The Portuguese earthquake of 1969 (number 34 in Table 1) has m_b of 7.3, the largest of any of the events in Table 1. The average T for this event was 1.77 sec; the Haskell model predicts that if m_b had been determined at 1 sec, it would be 0.5 smaller. A systematic variation of T as a function of m_b could account for part of the difference between the theoretical curve and observations. Another possible explanation of the difference may be heterogeneity of the source mechanism. This possibility is discussed later in more detail.

High-Frequency Spectra

The Haskell model, which has ω^{-3} high-frequency decay, moment proportional to L^3 and "corner frequency", ω_c, (for fixed source-receiver geometry, source similarity and source mechanism) proportional to L^{-1}, is a particular member of a general class of models having those properties. Following an argument first suggested by Savage (1972), note that for many source models the area radiating energy to a far-field observer will appear to grow as t^2 and dislocation from that area will grow linearly with t. The far-field

pulse, which is the time derivative of the moment function will grow as t^2, giving (Bracewell, 1965, p. 144) ω^{-3} high-frequency spectral decay (assuming the t^2 onset is the most abrupt discontinuity). Many models will also have a "corner frequency" proportional to L^{-1}, where L is some characteristic source dimension of that model. Finally, most models give $M_o \sim L^3$, where L is a source dimension. For all models meeting the above three requirements, high-frequency spectral amplitudes will behave as

$$A(\omega) \sim M_o(\omega_c/\omega)^3 \sim L^3(L^{-1}/\omega)^3 \sim \omega^{-3}.$$

Thus, all events with fixed geometry and source type will share a common high-frequency asymptote which is independent of L. Therefore, the conclusion that m_b, and for much larger events, M_S, will have a maximum value, applies to a more general class of models. For example, Minster (1973) derived m_b-M_S curves (with a similar shape to the curve from

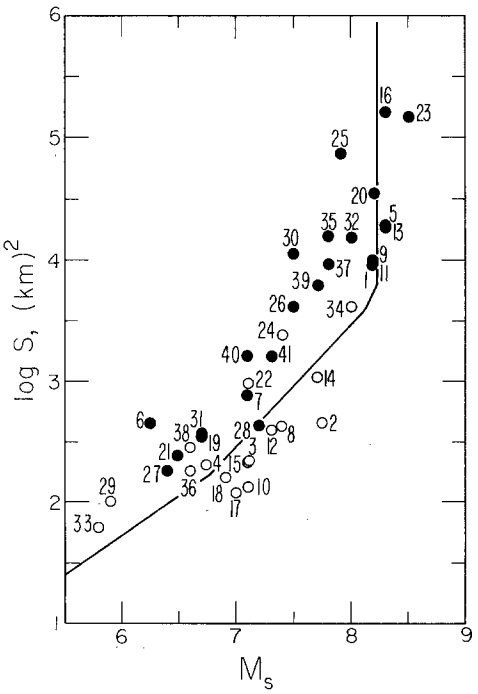

FIG. 6. M_S versus log S data with theoretical curve from Haskell model.

the Haskell model in Figure 5) from an Archambeau type (volume) source (also ω^{-3} falloff), although he did not calibrate them against m_b-M_S data. Minster's results also predict maximum values of m_b and M_S.

Many investigators, such as Richards (1973), Dahlen (1974), Sato and Hirasawa (1973) and Madariaga (1975) have outlined crack models for which the initial rupture contributes an ω^{-3} high-frequency spectrum while a "stopping phase" caused by simultaneous cessation of fracture everywhere on the fault contributes ω^{-2} or $\omega^{-5/2}$ and therefore dominates the high-frequency spectrum. If such models are applicable, m_b, which is based on the initial rupture, would still have a maximum value, but M_S would not.

M_S versus fault area. Figure 6 is a plot of fault area, S (taken from Table 1), and M_S. The predicted M_S-log S curve derived from (21) to (25) agrees quite well with the data. Note that the theoretical curve has four different segments. For small earthquakes, up to $M_S = 6.76$, the slope is $\frac{2}{3}$. From $M_S = 6.76$ to $M_S = 8.12$, the region in which most moderately

large earthquakes are clustered, the slope is 1. There is a small section for which the slope is 2, from $M_S = 8.12$ to $M_S = 8.22$. After $M_S = 8.22$, the largest value of M_S for this calibration of the Haskell model, the slope is infinite (e.g., S increases with no further increase in magnitude).

There is a systematic difference between the interplate (closed circles) and intraplate (open circles) in Figure 6. Half of the intraplate events fall below the predicted $M_S - \log S$ curve, while nearly all interplate earthquakes are above the curve. Kanamori and Anderson (1975b) showed that, at least in the region with slope one, this meant intraplate events had a higher apparent stress.

Utsu and Seki (1954) found the empirical relation $\log S = 1.02\,M - 4.01$. Their M is Japan Meteorological Agency (JMA) magnitude which is roughly equivalent to M_S, and S is in square kilometers. For the unit slope part of the $M_S - \log S$ curve in Figure 6 ($M_S > 6.76$)

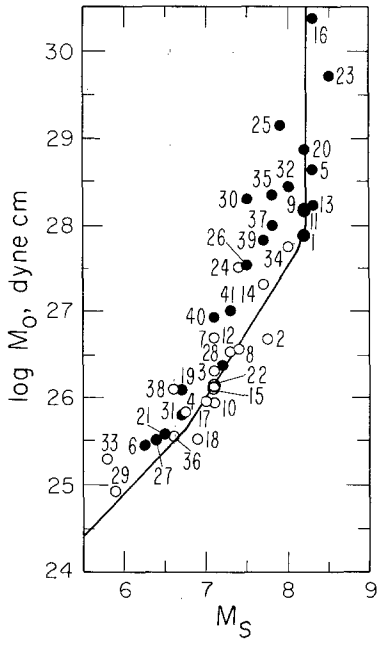

FIG. 7. M_S versus log M_0 data with theoretical curve from Haskell model.

the Utsu-Seki relation predicts about five times the fault area. This may be due to the way Utsu and Seki apparently determined fault area. They used an area encompassing nearly all of the aftershocks, rather than the one-day aftershock zone which seems to give much better agreement with observed fault dimensions for earthquakes on continents. Båth and Duda (1964) proposed the relation $\log S = 1.21\,M_S - 5.05$, based on a study of six earthquakes from different regions. Båth and Duda used S as aftershock area (in square kilometers) not fault-plane area, so this is basically similar to Utsu and Seki's result. Cinnery (1969) summarizes a number of efforts to find a single linear relation between M_S and the logarithm of other fault parameters.

M_S versus moment. The data of Kanamori and Anderson (1975b) show that $\Delta\sigma = 50$ bars is a good average, about halfway between values for interplate and intraplate events. Using $\Delta\sigma = 50$ and (15), we find moment (in dyne centimeters) is related to fault length (in kilometers by $M_o = (7.26 \times 10^{21})\,L^3$ or $\log M_o = 21.9 + 3 \log L$. It was shown above that $M_S \sim n \log L$, where n varies between 0 and 3, as can be seen from the surface-wave spectra

in Figure 4. Therefore, for small earthquakes the M_S:$\log M_o$ slope is one: for very large events ($M_S \sim$ constant) the slope is infinite (M_o increases but M_S is already at a maximum).

The $\log M_o$-M_S data from Table 1 are plotted in Figure 7. Most of the moderate-sized events (M_S from 6.76 to 8.11) fall on the slope 1.5 portion of the curve ($\log M_o \sim \frac{3}{2} M_S$). This part of the curve corresponds to cases where 20-sec spectral amplitudes are measured on the ω^{-1} part of the spectrum. Because the corner frequency for width is only slightly greater than that for rise time, the slope 3 ($M_o \sim 3 \log M_S$) region is very small, extending only from $M_S = 8.12$ to $M_S = 8.22$. Beyond that, slope is infinite. The data agree quite well with the theoretical curve. As in Figure 6, intraplate events tend to have smaller M_o for a given M_S, corresponding to higher apparent stress.

Aki (1972) showed that his ω-square model also agreed well with M_S versus $\log M_o$ data. Brune and co-workers (Brune and King, 1967; Brune, 1968; and Brune and Engen, 1969) presented a magnitude scale based on 100-sec surface-wave amplitude. They then assumed $\log M_o \sim \log A(100)$ and fit two segments, each with slope 1, to the data. Because of their different definition of M_o, their results cannot be directly compared to this paper.

Data in this section show that when M_o is larger than about 10^{28} dyne cm, M_S reaches its maximum value. It is important to consider this when discussing the "maximum credible earthquake" likely to occur in a particular area. The earthquake size may be specified in terms of M_S for most earthquakes, but when the moment approaches 10^{28}, magnitude no longer is a valid parameter for specifying earthquake size. Whenever the maximum credible earthquake is in this range, e.g., as is probably the case in discussing the Alaskan pipeline, moment, not M_S, should be the parameter used.

Spectral Ratios of Similar Events

Berckhemer (1962) studied spectral ratios of earthquakes with roughly the same location and mechanism. In theory, the spectral ratio method eliminates the effect of earth structure and leaves only effects due to the difference in source spectra. Aki (1967) used Berckhemer's data to determine the relation between M_S and corner period for the ω-square and ω-cube models.

Berckhemer's (1962) original data and Aki's (1967) theoretical curves are shown in Figure 8 together with the theoretical curve from the model in this paper. Both models seem to agree fairly well with the data. Perhaps Aki's fits slightly better. Berckhemer presented six pairs of spectra, of which only four are presented here. The remaining two pairs used smaller earthquakes, involving mostly short-period data, which probably are less reliable. No attempt at fitting these two pairs was made.

Tsujiura (1973) published spectral ratio data for many pairs of earthquakes. Most of his events could be fit by both Aki's (1967) ω-square model or Aki's (1972) version of Brune's "ω-model", although usually one model or the other fit somewhat better. There were, however, two pairs of events from the Aleutians which had spectral ratios that were unusually flat and could not be fit by either model. Tsujiura's spectral ratio data have not yet been compared to the model in this paper.

Discussion

The Haskell model with parameters (21) to (24) is in general agreement with m_b-M_S data (Figure 5), $M_S - \log S$ data (Figure 6), $M_S - \log M_o$ data (Figure 7) and spectral ratio data (Figure 8). The most serious discrepancy between the data and the model comes in Figure 5. On one hand, the maximum value of m_b is probably several tenths too small. On the

other, the data seem to have a slope of about one up to $m_b = 5\frac{1}{4}$, while the curve from the model has slope one only up to $m_b = 4.19$.

This phenomenon could be explained if most earthquakes are complex sources with the first burst of energy coming from a smaller, substantially higher stress drop source, than the average of the whole earthquake. If this is the case, then m_b would be measured on a flat or flatter part of the spectrum than one would expect for the earthquake as a whole.

Burdick and Mellman (1976) have suggested that for the Borrego earthquake of 1968 most of the body-wave energy came from a source region with radius of 8 km, giving about half the area shown in Table 1. Since they also found a higher moment, 0.112×10^{27} dyne cm, their stress drop, 96 bars, is about 4 times the value in Table 1, taken from Hanks and Wyss (1972). Tucker and Brune (1975) also suggested that sources showed a smaller high stress drop event superimposed on the overall average event. The m_b-M_S data in Figure 5

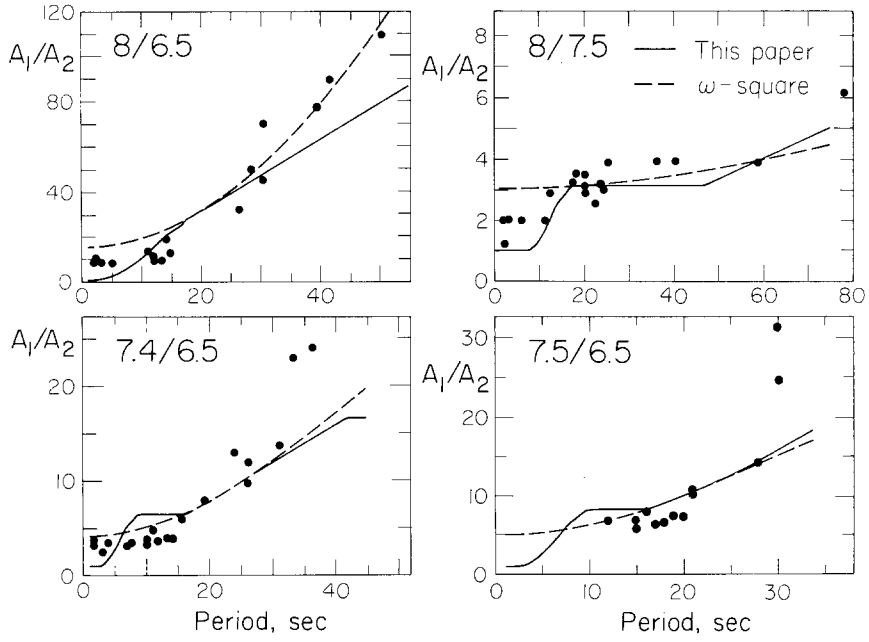

FIG. 8. Spectral ratios of similar earthquakes from Berckhemer (1962). Numbers above each figure are magnitudes of the larger and smaller of the events. Dashed line is ω-square model and solid line is model from this paper.

agree with the possibility of the initial fracture having higher stress drop than the bulk event, but certainly do not prove that this happens. Other explanations are equally admissible.

CONCLUSIONS

The following scaling relations relating width and rise time to length and fault area have been given

$$L = 2W$$
$$\tau = 16S^{1/2}/(7\pi^{3/2}\beta).$$

The relation for rise time was derived from the assumption that static stress drop and

dynamic effective stress are equal; agreement of theoretical rise times with the data tends to support that assumption.

Averages of observed rupture velocities show that $v_R = 0.72\beta$.

The Haskell model predicts that magnitude will reach an upper limit regardless of further increases in fault length and seismic moment. Moment, rather than magnitude should be used to discuss the possible size of great earthquakes.

The "source spectrum" from any source model is a function of apparent (phase) velocity of the mode or phase being considered, as well as of azimuth and source parameters. It is incorrect to speak of a single "source spectrum."

Theoretical relations between m_b and M_S from the Haskell model are

$$\begin{aligned} m_b &= M_S + 1.33 && M_S < 2.86 \\ m_b &= \tfrac{2}{3}M_S + 2.28 && 2.86 < M_S < 4.90 \\ m_b &= \tfrac{1}{3}M_S + 3.91 && 4.90 < M_S < 6.27 \\ m_b &= 6.00 && 6.27 < M_S. \end{aligned}$$

M_S and fault area (in square kilometers) are related by

$$\begin{aligned} \log S &= \tfrac{2}{3}M_S - 2.28 && M_S < 6.76 \\ \log S &= M_S - 4.53 && 6.76 < M_S < 8.12 \\ \log S &= 2M_S - 12.65 && 8.12 < M_S < 8.22 \\ M_S &= 8.22 && S > 6080\ \text{km}^2 \end{aligned}$$

if $L = 2W$ is used.

If we assume a stress drop of 50 bars, then $\log M_o$ (in dyne centimeters) and M_S are related by

$$\begin{aligned} \log M_o &= M_S + 18.89 && M_S < 6.76 \\ \log M_o &= \tfrac{3}{2}M_S + 15.51 && 6.76 < M_S < 8.12 \\ \log M_o &= 3M_S + 3.33 && 8.12 < M_S < 8.22 \\ M_S &= 8.22 && \log M_o > 28. \end{aligned}$$

These scaling relations fit observed data quite well. They should not be used to determine the value of a parameter for any individual earthquake, since these "averages", and the assumptions made to derive them, are not exactly correct for any single event.

A review of work by Gutenberg and Richter reveals that their m_b-M_S relation was derived from m_b data at mostly 5- or 10-sec period. Models such as Aki's (1967) ω-square model which fit theoretical 1 sec m_b data to the Gutenberg-Richter relation are probably in error.

Acknowledgments

I have benefited greatly from discussions and comments on the manuscript by Don Anderson, Jerry Frazier, Tom Hanks, David Harkrider, Don Helmberger, Hiroo Kanamori, Dan Kosloff and Kunihiko Shimazaki. Hiroo Kanamori and Don Anderson kindly made their data and manuscript available prior to publication. Hiroo Kanamori called the discrepancy between modern and classical m_b data to my attention. I sincerely thank the anonymous reviewer for his constructive criticism. This research was supported by the Advanced Research Projects Agency of the Department of Defense and was monitored by the Air Force Office of Scientific Research under Contract F44620-72-C-0078, and by U.S. Geological Survey Contract 14-08-0001-15273.

References

Abe, K. (1972a). Lithospheric normal faulting beneath the Aleutian trench, *Phys. Earth. Planet Interiors* **5**, 190–198.

Abe, K. (1972b). Mechanisms and tectonic implications of the 1966 and 1970 Peru earthquakes, *Phys. Earth Planet Interiors* **5**, 367–379.

Abe, K. (1973). Tsunami and mechanism of great earthquakes, *Phys. Earth Planet Interiors* **7**, 143–153.

Abe, K. (1974a). Fault parameters determined by near- and far-field data: The Wakasa Bay earthquake of March 26, 1963, *Bull. Seism. Soc. Am.* **64**, 1369–1382.

Abe, K. (1974b). Seismic displacement and ground motion near a fault: The Saitama earthquake of September 21, 1931, *J. Geophys. Res.* **79**, 4393–4399.

Abe, K. (1975a). Re-examination of the fault model for the Niigata earthquake of 1964, *J. Phys. Earth* **23**, 349–366.

Abe, K. (1975b). Determination of static and dynamic fault parameters: The Saitama earthquake of July 1, 1968, *Tectonophysics* **27**, 223–238.

Abe, K. (1975c). Reliable estimation of the seismic moment of large earthquakes, *J. Phys. Earth* **23**, 381–390.

Aki, K. (1967). Scaling law of seismic spectrum, *J. Geophys. Res.* **72**, 1217–1231.

Aki, K. (1972). Scaling law of earthquake source time function, *Geophys. J.* **31**, 3–25.

Anderson, J. (1974). A dislocation model for the Parkfield earthquake, *Bull. Seism. Soc. Am.* **64**, 671–686.

Ando, M. (1974). Faulting in the Mikawa earthquake of 1945, *Tectonophysics* **22**, 173–186.

Andrews, D. J. (1975). From moment to anti-moment: Plane-strain models of earthquakes that stop, *Bull. Seism. Soc. Am.* **65**, 163–182.

Archambeau, C. B. (1975). Studies of multiple seismic events, *Final Report, ACDA/ST220*, Seismological Laboratory, California Institute of Technology, Pasadena, California 91125.

Archuleta, R. and J. N. Brune (1975). Surface strong motion associated with a stick-slip event in a foam rubber model of earthquakes, *Bull. Seism. Soc. Am.* **65**, 1059–1071.

Båth, M. (1969). Handbook on earthquake magnitude determinations, Seismological Institute, Uppsala, *VESIAC Special Report, 7885-36-X* (second edition).

Båth, M. and S. J. Duda (1964). Earthquake volume, fault plane area, seismic energy, strain, deformation and related quantities, *Ann. Geofis.* (Rome), **17**, 353–368.

Ben-Menahem, A. (1961). Radiation of seismic surface-waves from finite moving sources, *Bull. Seism. Soc. Am.* **51**, 401–435.

Ben-Menahem, A. (1962). Radiation of seismic body waves from a finite moving source in the earth, *J. Geophys. Res.* **67**, 345–350.

Berckhemer, H. (1962). Die Ausdehnung der Bruchflache im Erdbebenherd und ihr Einfluss auf das seismische Wellenspektrum, *Beitr. Geophysik.* **71**, 5–26.

Boore, D. M. and M. D. Zoback (1974). Two-dimensional kinematic fault modeling of the Pacoima Dam strong-motion recordings of the February 9, 1971, San Fernando earthquake, *Bull. Seism. Soc. Am.* **64**, 555–570.

Bracewell, R. (1965). *The Fourier transform and its applications*, McGraw-Hill, New York.

Brune, J. N. (1968). Seismic moment, seismicity and rate of slip along major fault zones, *J. Geophys. Res.* **73**, 777–784.

Brune, J. N. (1970). Tectonic stress and the spectra of seismic shear waves from earthquakes, *J. Geophys. Res.* **75**, 4997–5009.

Brune, J. N. (1971). Correction, *J. Geophys. Res.* **76**, 5002.

Brune, J. N. and C. R. Allen (1967). A low stress-drop, low-magnitude earthquake with surface faulting: The Imperial, California earthquake of March 4, 1966, *Bull. Seism. Soc. Am.* **57**, 501–514.

Brune, J. N. and G. R. Engen (1969). Excitation of mantle Love waves and definition of mantle wave magnitude, *Bull. Seism. Soc. Am.* **59**, 923–933.

Brune, J. N. and C. Y. King (1967). Excitation of mantle Rayleigh waves of period 100 seconds as a function of magnitude, *Bull. Seism. Soc. Am.* **57**, 1355–1365.

Burdick, L. J. and G. R. Mellman (1976). Inversion of the body waves from the Borrego Mountain earthquake to the source mechanism, *Bull. Seism. Soc. Am.* **66**, 1485–1499.

Burridge, R. and L. Knopoff (1964). Body force equivalents for seismic dislocations, *Bull. Seism. Soc. Am.* **54**, 1875–1888.

Burridge, R. and J. R. Willis (1969). The self-similar problem of the expanding elliptical crack in an anisotropic solid, *Proc. Cambridge Phil. Soc.* **66**, 443–468.

Byerly, P. and J. DeNoyer (1958). Energy in earthquakes as computed for geodetic observations, in *Contributions in Geophysics, In Honor of Beno Gutenberg*, H. Benioff, M. Ewing, B. F. Howell and F. Press, Editors, Pergamon Press, New York, 17–35.

Chinnery, M. A. (1964). The Earth's crust under horizontal shear stress, *J. Geophys. Res.* **69**, 2085–2089.

Chinnery, M. A. (1969). Earthquake magnitude and source parameters, *Bull. Seism. Soc. Am.* **59**, 1969–1982.

Dahlen, F. A. (1974). On the ratio of *P*-wave to *S*-wave corner frequencies for shallow earthquake sources, *Bull. Seism. Soc. Am.* **64**, 1159–1180.

de Hoop, A. T. (1958). Representation theorems for the displacement in an elastic solid and their application to elastodynamic diffraction theory, *Thesis*, Technische Hogeschool, Delft.

Evernden, J. F. (1975). Further studies on seismic discrimination, *Bull. Seism. Soc. Am.* **65,** 359–391.

Fukao, Y. (1973). Thrust faulting at a lithospheric plate boundary: The Portugal earthquake of 1969, *Earth Planet. Sci. Lett.* **18,** 205–216.

Gutenberg, B. (1945). Amplitudes of *P*, *PP* and *S* and magnitude of shallow earthquakes, *Bull. Seism. Soc. Am.* **35,** 57–69.

Gutenberg, B. and C. F. Richter (1942). Earthquake magnitude, intensity, energy and acceleration, *Bull. Seism. Soc. Am.* **32,** 163–191.

Gutenberg, B. and C. F. Richter (1956). Magnitude and energy of earthquakes, *Ann. Geofis.* (Rome), **9,** 1–15.

Hanks, T. C. and M. Wyss (1972). The use of body wave spectra in the determination of seismic-source parameters, *Bull. Seism. Soc. Am.* **62,** 561–589.

Hanson, M. E., A. R. Sanford and R. J. Shaffer (1974). A source function for a dynamic brittle unilateral shear fracture, *Geophys. J.* **38,** 365–376.

Harkrider, D. G. (1964). Surface waves in multilayered elastic media, 1. Rayleigh and Love waves from buried sources in a multilayered elastic half-space, *Bull. Seism. Soc. Am.* **54,** 627–679.

Harkrider, D. G. (1970). Surface waves in multilayered elastic media. Part II. Higher mode spectra and spectral ratios from point sources in plane layered earth models, *Bull. Seism. Soc. Am.* **60,** 1937–1987.

Haskell, N. A. (1964). Total energy and energy spectral density of elastic wave radiation from propagating faults, *Bull. Seism. Soc. Am.* **54,** 1811–1841.

Haskell, N. A. (1966). Total energy and energy spectral density of elastic wave radiation from propagating faults. Part II. A statistical fault model, *Bull. Seism. Soc. Am.* **56,** 125–140.

Haskell, N. A. (1969). Elastic displacements in the near-field of a propagating fault, *Bull. Seism. Soc. Am.* **59,** 865–908.

Hirasawa, T. and W. Stauder (1965). On the seismic body waves from a finite moving source, *Bull. Seism. Soc. Am.* **55,** 237–262.

Kanamori, H. (1970a). Synthesis of long-period surface waves and its application to earthquake source studies—Kurile Islands earthquake of October 13, 1963, *J. Geophys. Res.* **75,** 5011–5027.

Kanamori, H. (1970b). The Alaska earthquake of 1964: Radiation of long-period surface waves and source mechanism, *J. Geophys. Res.* **75,** 5029–5040.

Kanamori, H. (1971a). Faulting of the great Kanto earthquake of 1923 as revealed by seismological data, *Bull. Earthquake Res. Inst., Tokyo Univ.* **49,** 13–18.

Kanamori, H. (1971b). Seismological evidence for a lithospheric normal faulting—the Sanriku earthquake of 1933, *Phys. Earth Planet. Interiors* **4,** 289–300.

Kanamori, H. (1971c). Focal mechanism of the Tokachi-Oki earthquake of May 16, 1968: Contortion of the lithosphere of a junction of two trenches, *Tectonophysics* **12,** 1–13.

Kanamori, H. (1972a). Tectonic implications of the 1944 Tonankai and 1946 Nankaido earthquakes, *Phys. Earth Planet. Interiors* **5,** 129–139.

Kanamori, H. (1972b). Determination of effective tectonic stress associated with earthquake faulting, the Tottori earthquake of 1943, *Phys. Earth Planet. Interiors* **5,** 426–434.

Kanamori, H. (1973). Mode of strain release associated with major earthquakes in Japan, *Ann. Rev. Earth Planet. Sci.* **1,** 213–239.

Kanamori, H. (1974). Long period ground motion in the epicentral area of major earthquakes, *Tectonophysics* **21,** 341–356.

Kanamori, H. and D. L. Anderson (1975a). Amplitude of the Earth's free oscillations and long period characteristics of the earthquake source, *J. Geophys. Res.* **80,** 1075–1078.

Kanamori, H. and D. L. Anderson (1975b). Theoretical basis of some empirical relations in seismology, *Bull. Seism. Soc. Am.* **65,** 1073–1095.

Kanamori, H. and J. J. Cipar (1974). Focal processes of the great Chilean earthquake May 22, 1960, *Phys. Earth Planet. Interiors* **9,** 128–136.

Kasahara, K. (1957). The nature of seismic origins as inferred from seismological and geodetic observations, 1, *Bull. Earthquake Res. Inst., Tokyo Univ.* **35,** 473–532.

Kawasaki, I. and Y. Suzuki (1974). Rise time and effective stress estimation from comparison of near field data with theoretical seismograms in a semi-infinite medium: The Sanriku earthquake of March 3, 1933, *J. Phys. Earth* **22,** 223–236.

Kawasaki, I. (1975). The focal processes of the Kita-Mino earthquake of August 19, 1961 and its relationship to a Quaternary fault, the Hatogayu-Koike fault, *J. Phys. Earth* **23,** 227–250.

Keiles-Borok, V. (1959). An estimation of the displacement in an earthquake source and of source dimensions, *Ann. Geofis.* (Rome), **12,** 205–214.

Langston, C. A. and D. V. Helmberger (1975). A procedure for modelling shallow dislocation sources, *Geophys. J.* **42,** 117–130.

Madariaga, R. (1975). Dependence of far-field radiation on source geometry (abstract), *Trans. Am. Geophys. Un.* **56,** 400–401.

Mikumo, T. (1969). Long-period *P* waveforms and the source mechanism of intermediate earthquakes, *J. Phys. Earth* **17,** 169–192.

Mikumo, T. (1973a). Faulting mechanism of the Gifu earthquake of September 9, 1969, and some related problems, *J. Phys. Earth* **21,** 191–212.

Mikumo, T. (1973b). Faulting processes of the San Fernando earthquake of February 9, 1971 inferred from static and dynamic near-field displacements, *Bull. Seism. Soc. Am.* **63,** 249–269.

Minster, J. B. (1973). *Elastodynamics of failure in a continuum*, Thesis, California Institute of Technology, Pasadena, California 91125.

Nagamune, T. (1972). Magnitudes estimated from body waves for great earthquakes (in Japanese), *Quart. J. Seism.* **47,** 1–8.

Richards, P. G. (1973). The dynamic field at a growing plane elliptical shear crack, *Intern. J. Solids Struct.* **9,** 843–861.

Richter, C. F. (1958). *Elementary Seismology*, W. H. Freeman, San Francisco.

Sato, R. (1972). Stress drop for a finite fault, *J. Phys. Earth* **20,** 397–407.

Sato, T. and T. Hirasawa (1973). Body wave spectra from propagating shear cracks, *J. Phys. Earth* **21,** 415–431.

Savage, J. C. (1972). Relation of corner frequency to fault dimensions, *J. Geophys. Res.* **77,** 3788–3795.

Savage, J. C. and L. M. Hastie (1966). Surface deformation associated with dip-slip faulting, *J. Geophys. Res.* **71,** 4897–4904.

Shimazaki, K. (1975). Nemuro-Oki earthquake of June 17, 1973: A lithospheric rebound at the upper half of the interface, *Phys. Earth Planet. Interiors* **9,** 314–327.

Trifunac, M. D. (1974). A three-dimensional dislocation model for the San Fernando, California, earthquake of February 9, 1971, *Bull. Seism. Soc. Am.* **64,** 149–172.

Trifunac, M. D. and F. E. Udwadia (1974). Parkfield, California, earthquake of June 27, 1966: A three-dimensional moving dislocation, *Bull. Seism. Soc. Am.* **64,** 511–533.

Tsai, Y. and K. Aki (1970). Source mechanism of the Truckee, California earthquake of September 12, 1966, *Bull. Seism. Soc. Am.* **60,** 1199–1208.

Tsuboi, C. (1956). Earthquake energy, earthquake volume, aftershock area, and strength of the earth's crust, *J. Phys. Earth* **4,** 63–66.

Tsujiura, M. (1973). Spectrum of seismic waves and its dependence on magnitude, *J. Phys. Earth* **21,** 373–391.

Tucker, B. E. and J. N. Brune (1975). Source mechanism and surface wave excitation for aftershocks of the San Fernando earthquake (preprint).

Udias, A. (1971). Source parameters of earthquakes from spectra of Rayleigh waves, *Geophys. J.* **22,** 353–376.

Udias, A. and A. L. Arroyo (1970). Body and surface wave study of source parameters of the March 15, 1964 Spanish earthquake, *Tectonophysics* **9,** 323–346.

Utsu, T. and A. Seki (1954). A relation between the area of aftershock region and the energy of main-shock (in Japanese), *J. Seism. Soc. Japan (Zisin)* **7,** 233–240.

Wu, F. T. and H. Kanamori (1973). Source mechanism of February 4, 1965, Rat Island earthquake, *J. Geophys. Res.* **78,** 6082–6092.

SEISMOLOGICAL LABORATORY
CALIFORNIA INSTITUTE OF TECHNOLOGY
PASADENA, CALIFORNIA 91125

DIVISION OF GEOLOGICAL AND PLANETARY SCIENCES
CONTRIBUTION NO. 2696

Manuscript received November 11, 1975